Electron-Beam Lithography

DOI: 10.1002/anie.201006560

Electron-Beam-Induced Deposition of Metallic Microstructures from a Molten-Salt Film on Conductive and Nonconductive Substrates**

*Vadym Halka, Matthias J. Schmid, Vsevolod Avrutskiy, Xinzhou Ma, and Rolf Schuster**

Lithographical processes are among the most important techniques for microfabrication, and applications range from chip fabrication to the structuring of micromechanical and microfluidic devices.[1] In many applications, metallic structures such as chip interconnects are obtained by a sequential process in which, for example, a polymer mask is first lithographically patterned and subsequently coated with metal. Direct, one-step creation of metallic nanostructures is limited to only a few processes. Although the electron-beam-induced deposition (EBID) of nanoscale structures from mostly gaseous organometallic precursors is well established,[2,3] the production of pure metal deposits was demonstrated only recently.[4] Solid metal salts were also used as precursors for the deposition of metal nanoparticles, which were, however, mostly very finely dispersed on the surface, due to the limited material supply by the thin salt film.[5,6] In addition local catalytic activity, induced by EBID of Fe or by electron irradiation of a SiO_x film, was employed for the local decomposition of a gaseous iron-containing precursor.[7] Similarly, electron- or ion-beam-induced surface defects can serve as nuclei for the electrochemical deposition of metals on a silicon surface.[8] Local electrochemical metal deposition by use of electrochemical scanning probes was also demonstrated.[9–12]

Herein we present an approach, in which a metal, in the present case silver, is deposited locally onto conductive and nonconductive substrates by irradiation of a micrometer-thin, molten-metal-salt film with a focused electron beam from a scanning electron microscope. The method is similar to the conventional EBID process; however, owing to the liquid, well-wetting electrolyte film, the supply of material is ensured also for rather thick metal structures. Furthermore, the electric conductivity of the electrolyte film allows the patterning of nonconductive surfaces. By changing the irradiation parameters, the morphology and thickness of the deposits can be varied from small nanoparticles to rather large microcrystallites and thick conductive structures.

Figure 1 shows checkerboard patterns of Ag nanoparticles deposited onto Si, Ta, and glass by irradiation of an about 1–3 μm thick molten $AgNO_3$ film at 260 °C with a 15 keV focused electron beam in a Hitachi S 450 scanning electron microscope (SEM). The bright areas of the checkerboard were repetitively scanned with a scan speed of 1 mm s^{-1} and 500 lines per bright square. For the patterning of the Si substrate shown in Figure 1a the beam current was 1 nA, yielding a total dose of approximately 6 mC cm^{-2}. The other patterns required similar doses. Ag nanoparticles grew along the trace of the electron beam; they stick so strongly to the surface that the salt film could be washed off after irradiation and the metal structures remained on the surface. Closer inspection of the irradiated areas revealed that rather regularly shaped crystallites formed on the surface with a broad size distribution ranging from a few 100 nm up to more than 1 μm. In the optical microscope the particles appeared metallic with the typical yellowish color of silver. Scanning Auger analysis of individual particles proved that they consisted of clean metallic silver. In particular, after the contaminations from sample handling were removed by gentle sputtering about 10 nm off the sample surface, carbon, oxygen, and nitrogen were below the detection limit of the scanning Auger spectrometer; this amounts to about 2 atom % for these elements. The presence of metallic silver was confirmed by cathodoluminescence measurements of the deposits upon 15 keV electron irradiation in a SEM.[13] The emission spectra of individual particles on Si exhibited an emission peak at about 330 nm, which could be attributed to deexcitation of Ag bulk plasmons, excited by the high-energy electrons.[14,15] Additional spectral features indicate excitation of localized plasmon modes of the Ag particles.

It has to be noted that Ag particles were found also in nonirradiated areas. However, their density was much less than the particle density in the irradiated areas. In addition, these particles were significantly smaller than the Ag particles in the irradiated areas. Similar amounts of Ag particles were found in blank experiments, where the $AgNO_3$ film was melted in the SEM stage without electron irradiation. We attribute these background particles to the precipitation of Ag colloids, which were present in the $AgNO_3$ film owing to contamination of the $AgNO_3$ salt or photoreduction by accidental exposure to light during the processing of the chemicals and during the preparation of the electrolyte layer. Since annealing of the film for up to three hours had only a minor influence on the number of background particles, thermal decomposition of $AgNO_3$ does not play a prominent role, although we cannot completely rule it out. It should be noted that the decomposition temperature of $AgNO_3$ of 444 °C[16] is almost 200 K higher than the temperature in our experiments.

Using a thin liquid electrolyte film is crucial for the success of the patterning process. Although after irradiation

[*] Dr. V. Halka, M. J. Schmid, V. Avrutskiy, X. Ma, Prof. Dr. R. Schuster
Karlsruhe Institute of Technology and DFG-Center for Functional Nanostructures, Kaiserstrasse 12, 76131 Karlsruhe (Germany)
E-mail: rolf.schuster@kit.edu

[**] This work was supported by the DFG Center for Functional Nanostructures, which we gratefully acknowledge. We also thank C. Kind and C. Feldmann for support with the elemental analysis of the particles.

Supporting information for this article is available on the WWW under http://dx.doi.org/10.1002/anie.201006560.

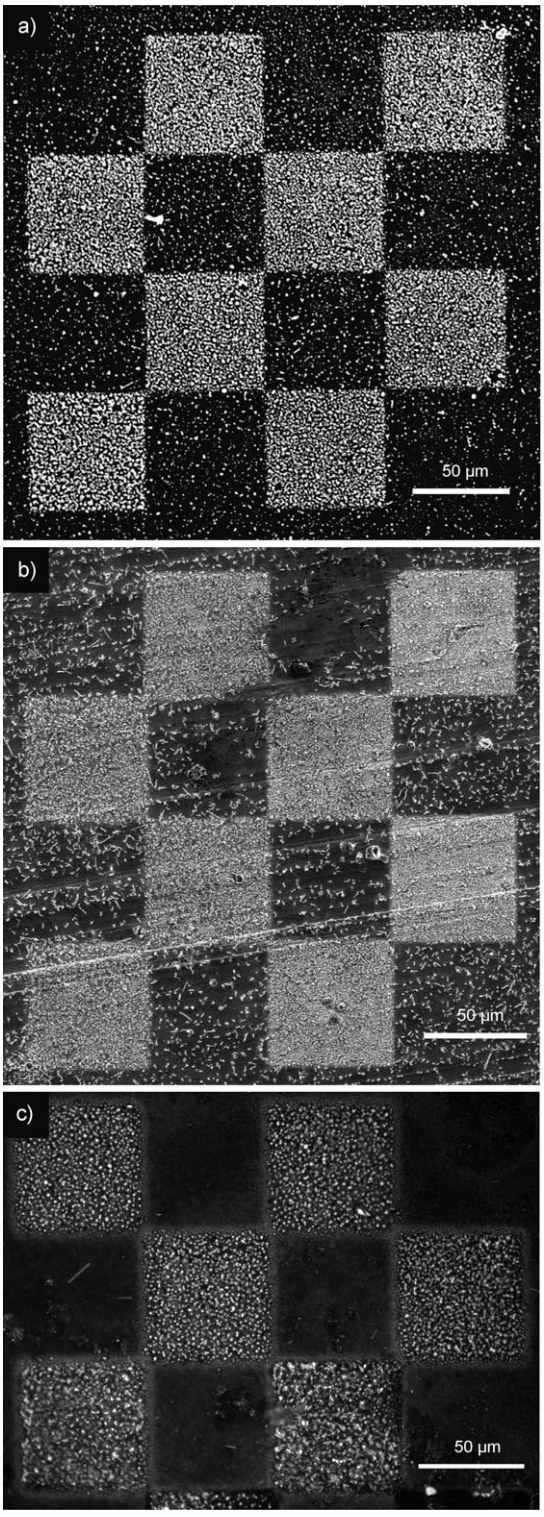

Figure 1. Checkerboard patterns of Ag particles on Si (a), Ta (b), and glass (c), formed by irradiation of a 1–3 µm thick liquid $AgNO_3$ film at 260 °C with a 15 keV electron beam in an SEM. The bright areas were scanned line by line with a beam current of 1 nA (a, b) and 0.6 nA (c) yielding total doses of 6 $mC\,cm^{-2}$. After irradiation, the $AgNO_3$ was washed off with water. The figures show SEM images (a, b) and an optical micrograph (c) of the surfaces after the salt film had been washed off.

of a solid $AgNO_3$ film the irradiated areas appeared grayish under the light microscope, no structures remained on the surface after the salt film had been washed off. Also melting of the salt film for about 10 min at 260 °C directly after electron-beam irradiation of a solid film did not lead to the formation of patterns on the surface. The grayish color under the light microscope implies that the reduction of silver ions was possible also in the solid film. However, the enhanced mobility in the liquid electrolyte film was mandatory for the nucleation and growth of silver particles and their attachment to the surface. Furthermore, substrate and deposited Ag were covered by the liquid electrolyte film throughout the experiment, such that material was constantly supplied by diffusion in the liquid. In addition, in situ SEM images of the molten $AgNO_3$ film showed no charging effects also for nonconductive substrates. A stable negative sample current was measured in all cases. We attribute this to the ionic conductivity of the film, together with electrochemical reactions at both the location of the beam and the stainless steel screw, which clamped and grounded the sample surface, in other words, the electrolyte film (see the Supporting Information). We suggest that surplus electrons in the film at the location of the electron beam eventually reduced NO_3^- or Ag^+ ions. Electrochemical counter reactions occurred at the stainless steel screw, probably upon decomposition of NO_3^- to N_2 and O_2 or oxidation of the screw. These electrochemical processes limited the potential drop between the irradiated area and the sample holder to a few volts, which prevented significant charging.

To derive further information on the deposition process, we studied the dependence of the morphology of the deposits on irradiation parameters like scan speed and total electron dose. Figure 2 a,b presents details of nanoparticle patterns on Si, which were obtained with the same total dose of 1.8 $mC\,cm^{-2}$ and the same beam current (0.3 nA), but with scan speeds differing by almost three orders of magnitude, and correspondingly different repetition times. Visual inspection already reveals that with faster scan speed larger particles were obtained, however, with a lower number density. Statistical analysis (see Figure S1 in the Supporting Information) resulted in average radii of 420 nm and 250 nm for the fast and slow scans, respectively. Within experimental error the deposited amount of Ag was about the same for both figures with a total yield of roughly 50 Ag atoms per primary electron.

The high yield of Ag atoms per primary electron excludes a direct reduction of silver by primary electrons and points instead to a radiation-chemical reaction. Pure thermal decomposition of $AgNO_3$ by local heating in the beam spot can be ruled out from our experiments, since variation of the scan speed by about three orders of magnitude had no significant influence on the Ag yield. In principle, radiation-chemical processes can be induced by primary, backscattered, or secondary electrons. At the present state of the experiments Presently we cannot identify the elementary processes responsible for the Ag production. Similar to conventional EBID processes, low-energy electrons may also play an important role.[2] However, owing to their short range in the molten film or solid substrate, Ag reduction by low-energy

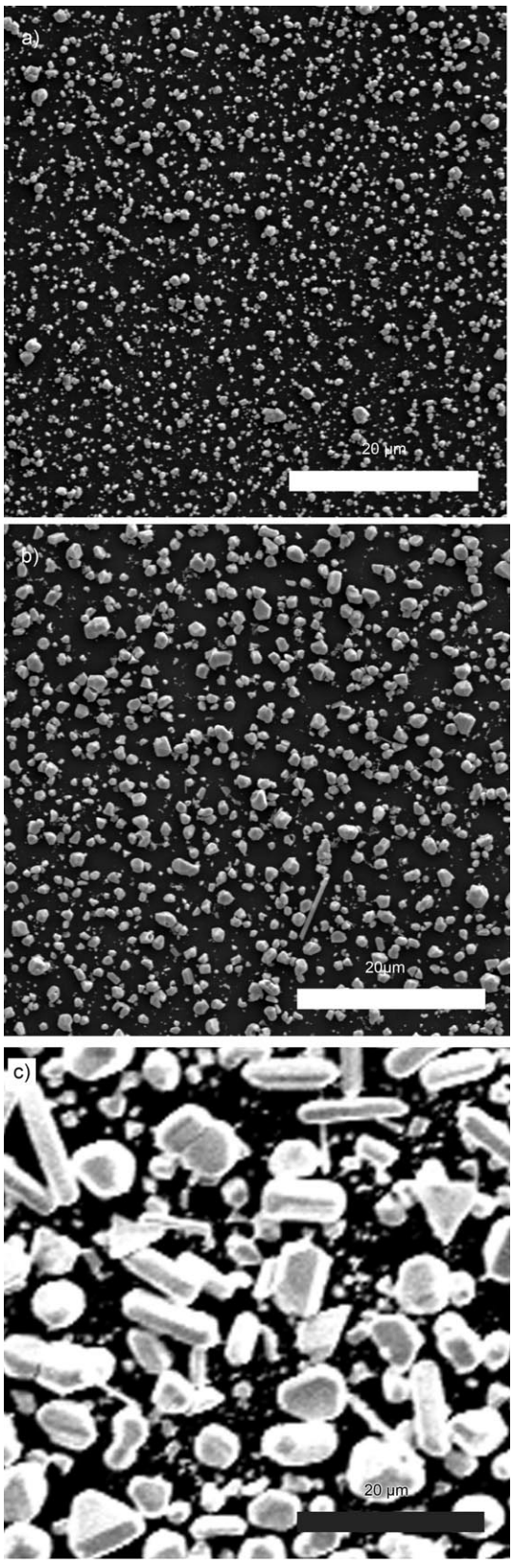

Figure 2. SEM images of Ag deposits on Si, obtained with varying irradiation parameters. The particles in (a, b) were deposited with the same dose of 1.8 mC cm^{-2} and the same beam current of 0.3 nA, but with scan rates of 2 mm s^{-1} (a) and 1000 mm s^{-1} (b). The repetition times were 2.5 s and 10 ms. In (c) the total dose was 12 mC cm^{-2} and the particles were obtained with a scan rate of 500 mm s^{-1} and a beam current of 1 nA.

electrons will be localized close to the traces of the high-energy electrons in the molten salt film. We are not aware of a study of the electron-induced radiation chemistry of $AgNO_3$, but Kaleciński studied the evolution of NO_2^- and O_2 upon the γ radiolysis of molten $AgNO_3$ at 240 °C.[17] He reported G values for NO_2^- and O_2 of 3.1 and 1.55 molecules per 100 eV deposited, respectively. Reaction products were found which were insoluble in water; however, their identity was not specified. Chen and Johnson studied the radiolysis of solid $AgNO_3$ by γ radiation at room temperature.[18] In accordance with the study on molten $AgNO_3$ they found the formation of NO_2^- and O_2. In addition, they reported the formation of traces of silver oxide. The occurrence of elementary Ag was not reported. However, our experiments were conducted at 260 °C, well above the decomposition temperature of bulk $AgNO_2$, which is 120 °C and above which $AgNO_2$ decomposes to metallic Ag and NO_2.[19] We therefore suggest that in our experiment the formation of Ag proceeds by formation of NO_2^- and O_2 by radiolysis of NO_3^- ions in the film, followed by thermal decomposition of the formed $AgNO_2$ to elementary Ag and NO_2. The formation of uncharged gaseous radiation-chemical products like NO_2 and O_2 is in accordance with experiments, where we measured the sample current upon varying the bias potential of a aperture with a diameter 1 mm hole, which was mounted 3 mm in front of the sample. With negative bias at the aperture, no current could be measured through the aperture, indicating that no positively charged reaction products leave the sample surface. With positive bias at the aperture, a current of about half the primary beam current was measured, which is much too small to explain the high yield of about 50 Ag atoms per primary electron. Instead, we attribute the aperture current upon positive bias to secondary electrons emitted from the sample surface. It should be noted that metallic Ag nanoparticles were also obtained by electron irradiation of AgI crystallites[5] and organic precursors;[20,21] however, the elementary reaction steps were not clarified in those studies.

The primary radiation-chemical process probably forms finely dispersed Ag atoms in the film, which tend to agglomerate into larger particles similar to the formation of Ag colloids in aqueous Ag^+ solutions upon γ irradiation[22] or upon electron irradiation of Ag^+-containing ionic liquids.[23,24] The strong dependence of the particle density on the scan speed is a direct consequence of the nucleation process. Upon slow scanning, the local Ag concentration built up in the beam spot is higher than that during fast scanning, which leads to a higher nucleation rate and therefore to more nuclei, in other words, a higher Ag particle density. Repetition of the pattern on a timescale of 10 ms, as employed for the fast scan in Figure 2b, could not compensate for the short residing time per point. From our data we cannot decide whether nucleation occurred in solution or at the surface. Radiation damage of the surface, however, did not play a prominent role for the particle density in Figures 2a and b, since the number of radiation defects is expected to be a function of the dose rather than the scan speed. Both experiments were conducted at the same total dose, but yielded different particle densities.

With increasing irradiation time, in other words, total dose, the Ag particles further grew and developed pro-

nounced facets (Figure 2c). The deposit in Figure 2c was formed with a total dose of 12 mC cm^{-2}, which is about 7 times higher than that of the patterns in Figure 2a,b. Besides triangular and hexagonal flat crystallites, elongated needles were also observed. The number of particles considerably decreased, compared to the earlier stages of the growth process. Apparently the particles ripened during the growth process and the crystals approached their thermal equilibrium shapes with large close-packed facets. It should be noted that the Ag-particle patterns were stable upon annealing at 260 °C for more than two hours in the presence of the liquid $AgNO_3$ film. We therefore attribute the coarsening of the pattern in Figure 2c to agglomeration of the particles and their reordering, rather than to Ostwald ripening, which would involve diffusional Ag transport across the substrate surface and would be strongly dependent on the annealing time. Similarly, Chen et al.[25] observed sintering and agglomeration of passivated gold nanoparticles under the electron beam. They observed the formation of a neck between adjacent particles indicating the diffusion of gold on the particle surface. Although the Ag particles in the present study were much larger, we propose that they ripened according to a similar mechanism after incidentally touching during the deposition process.

By proper choice of the irradiation conditions—at high doses and high current densities or short repetition times—compact, dense Ag structures could also be formed. Figure 3a shows five lines, obtained with a scan speed of 60 mm s^{-1}, a beam current of 1 nA, a repetition time of 500 µs, and 3×10^5 repetitions. Similarly, the conductive pattern in Figure 3b was scanned line by line with a beam current of 36 nA and a total dose of 34 mC cm^{-2}. The height of this pattern was 8 µm, reflecting the good wetting behavior of liquid $AgNO_3$ and the effective diffusional supply of the precursor.

In conclusion, a thin liquid electrolyte film can serve as the precursor for the direct electron-beam-induced deposition of metal on conductive and nonconductive substrates, owing to the ionic conductivity of the film. Mass transport in the film was the key for nucleation and growth of Ag crystallites which were strongly attached to the substrate surface. In the present study the precision of the structures was of the order of the thickness of the electrolyte film, which is conceivable from the nucleation and growth process of the Ag crystallites. Better defined patterns should be available by further reducing the thickness of the film, however, at the expense of a lower yield. Variation of the irradiation parameters like beam current and scan speed had pronounced influence on the morphology of the deposits, which ranged from isolated nanocrystallites to extended continuous and thick structures. In principle it should be possible to substitute the molten $AgNO_3$ film with other liquid metal salts. Also the use of electrolytes based on ionic liquids as solvents for metal salts may widen the range of available materials.

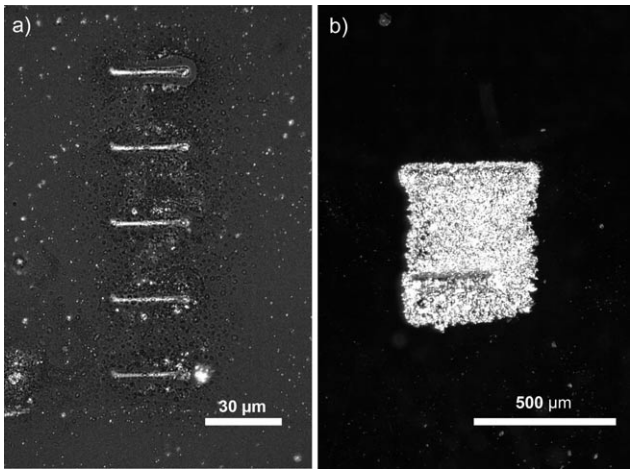

Figure 3. Optical micrographs of a) five compact lines and b) an 8 µm high conductive Ag pad on glass.

Received: October 19, 2010
Revised: March 1, 2011
Published online: April 14, 2011

Keywords: electron-beam lithography · nanoparticles · nanostructures · surface chemistry

[1] *Handbook of Microlithography, Micromachining, & Microfabrication*, *Vols. 1 and 2* (Ed.: P. Rai-Choudhury), SPIE Optical Engineering Press, Bellingham, WA, **1997**.
[2] W. F. van Dorp, C. W. Hagen, *J. Appl. Phys.* **2008**, *104*, 081301.
[3] S. J. Randolph, J. D. Fowlkes, P. D. Rack, *Crit. Rev. Solid State Mater. Sci.* **2006**, *31*, 55.
[4] T. Lukasczyk, M. Schirmer, H.-P. Steinrück, H. Marbach, *Small* **2008**, *4*, 841.
[5] J.-O. Malm, G. Schmid, B. Morun, *Philos. Mag. A* **1991**, *63*, 487.
[6] Y.-H. Pai, H.-F. Huang, Y.-C. Chang, C.-C. Chou, F.-S. Shieu, *J. Power Sources* **2006**, *159*, 878.
[7] A.-M. Walz, M. Schirmer, F. Vollnhals, T. Lukasczyk, H.-P. Steinrück, H. Marbach, *Angew. Chem.* **2010**, *122*, 4774; *Angew. Chem. Int. Ed.* **2010**, *49*, 4669.
[8] P. Schmuki, *Mater. Sci. Forum* **2006**, *512*, 129.
[9] A. J. Bard, M. V. Mirkin, *Scanning Electrochemical Microscopy*, Marcel Dekker, New York, **2001**.
[10] D. Hofmann, W. Schindler, J. Kirschner, *Appl. Phys. Lett.* **1998**, *73*, 3279.
[11] D. M. Kolb, R. Ullmann, T. Will, *Science* **1997**, *275*, 1097.
[12] R. Schuster, V. Kirchner, P. Allongue, G. Ertl, *Science* **2000**, *289*, 98.
[13] X. Ma, R. Schuster, *J. Electroanal. Chem.* **2011**, DOI: 10.1016/j.jelechem.2011.01.046.
[14] P. Chaturvedi, K. H. Hsu, A. Kumar, K. H. Fung, J. C. Mabon, N. X. Fang, *ACSNano* **2009**, *3*, 2965.
[15] H. Raether, *Excitation of Plasmons and Interband Transitions by Electrons*, Springer, New York, **1980**.
[16] *CRC Handbook of Chemistry and Physics*, 85th ed., (Ed.: D. L. Linde), CRC, New York, **2004**.
[17] J. Kalechiński, *Int. J. Radiat. Phys. Chem.* **1972**, *4*, 171.
[18] T.-H. Chen, E. R. Johnson, *J. Phys. Chem.* **1962**, *66*, 2249.
[19] K. C. Patil, R. K. Gosavi, C. N. R. Rao, *Inorg. Chim. Acta* **1967**, *1*, 155.
[20] S.-E. Kim, J.-U. Kim, Y. H. Han, B. C. Lee, J.-C. Lee, *J. Nanosci. Nanotechnol.* **2008**, *8*, 5212.
[21] S. Kinge, M. Crego-Calama, D. Reinhoudt, *New J. Chem.* **2008**, *32*, 2071.
[22] A. Henglein, M. Giersig, *J. Phys. Chem. B* **1999**, *103*, 9533.
[23] A. Imanishi, M. Tamura, S. Kuwabata, *Chem. Commun.* **2009**, 1775.
[24] S. A. Meiss, M. Rohnke, L. Kienle, S. Z. E. Abedin, F. Endres, J. Janek, *ChemPhysChem* **2007**, *8*, 50.
[25] Y. Chen, R. E. Palmer, J. P. Wilcoxon, *Langmuir* **2006**, *22*, 2851.

